

# Nature of magnetic excitations in superconducting $\text{BaFe}_{1.9}\text{Ni}_{0.1}\text{As}_2$

Mengshu Liu,<sup>1</sup> Leland W. Harriger,<sup>1</sup> Huiqian Luo,<sup>2</sup> Meng Wang,<sup>2,1</sup> R. A. Ewings,<sup>3</sup> T. Guidi,<sup>3</sup> Hyowon Park,<sup>4</sup> Kristjan Haule,<sup>4</sup> Gabriel Kotliar,<sup>4</sup> S. M. Hayden,<sup>5</sup> and Pengcheng Dai<sup>1,2</sup>

<sup>1</sup> *Department of Physics and Astronomy, The University of Tennessee, Knoxville, Tennessee 37996-1200, USA*

<sup>2</sup> *Beijing National Laboratory for Condensed Matter Physics,*

*Institute of Physics, Chinese Academy of Sciences, Beijing 100190, China*

<sup>3</sup> *ISIS Facility, Rutherford Appleton Laboratory, Chilton, Didcot, Oxfordshire OX11 0QX, UK*

<sup>4</sup> *Department of Physics, Rutgers University, Piscataway, NJ 08854, USA*

<sup>5</sup> *H. H. Wills Physics Laboratory, University of Bristol, Tyndall Avenue, Bristol, BS8 1TL, UK*

Since the discovery of the metallic antiferromagnetic (AF) ground state near superconductivity in iron-pnictide superconductors [1–3], a central question has been whether magnetism in these materials arises from weakly correlated electrons [4, 5], as in the case of spin-density-wave in pure chromium [6], requires strong electron correlations [7], or can even be described in terms of localized electrons [8, 9] such as the AF insulating state of copper oxides [10]. Here we use inelastic neutron scattering to determine the absolute intensity of the magnetic excitations throughout the Brillouin zone in electron-doped superconducting  $\text{BaFe}_{1.9}\text{Ni}_{0.1}\text{As}_2$  ( $T_c = 20$  K), which allows us to obtain the size of the fluctuating magnetic moment  $\langle m^2 \rangle$ , and its energy distribution [11, 12]. We find that superconducting  $\text{BaFe}_{1.9}\text{Ni}_{0.1}\text{As}_2$  and AF  $\text{BaFe}_2\text{As}_2$  [13] both have fluctuating magnetic moments  $\langle m^2 \rangle \approx 3.2 \mu_B^2$  per Fe(Ni), which are similar to those found in the AF insulating copper oxides [14, 15]. The common theme in both classes of high temperature superconductors is that magnetic excitations have partly localized character, thus showing the importance of strong correlations for high temperature superconductivity [16].

In the undoped state, iron pnictides such as  $\text{BaFe}_2\text{As}_2$  form a metallic low-temperature orthorhombic phase with the AF structure as shown in Fig. 1a [17]. Inelastic neutron scattering measurements have mapped out spin waves throughout the Brillouin zone in the AF orthorhombic and paramagnetic tetragonal phases [13]. Upon Co- and Ni-doping to induce optimal superconductivity via electron doping, the orthorhombic structural distortion and static AF order in  $\text{BaFe}_2\text{As}_2$  are suppressed and the system becomes tetragonal and paramagnetic at all temperatures [18]. In previous inelastic neutron scattering experiments on optimally electron-doped  $\text{Ba}(\text{Fe}, \text{Co}, \text{Ni})_2\text{As}_2$  superconductors [11, 12, 19–22], spin excitations up to  $\sim 120$  meV were observed. However, the lack of spin excitations data at higher energies in absolute units precluded a comparison with spin waves in undoped  $\text{BaFe}_2\text{As}_2$ . Only the absolute intensity measurements in the entire Brillouin zone can reveal the effect of electron-doping on the overall spin excitations spectra and allow a direct comparison with the results in the AF insulating copper oxides [14, 15]. For the experiments, we chose to study well-characterized electron-doped  $\text{BaFe}_{1.9}\text{Ni}_{0.1}\text{As}_2$  [20, 22] because large single crystals were available [23] and their properties are similar to Co-doped  $\text{BaFe}_2\text{As}_2$  [11, 12, 19, 21, 24].

By comparing spin excitations in  $\text{BaFe}_{1.9}\text{Ni}_{0.1}\text{As}_2$  and  $\text{BaFe}_2\text{As}_2$  throughout the Brillouin zone, we were able to probe how electron-doping and superconductivity affect the overall spin excitations spectra. We demonstrate that while the low-energy spin excitations are affected, the high-energy excitations show a very weak temperature and doping dependence. Comparison of our results with various theories suggests that neither a fully itinerant nor a localized picture explains the magnetic excitation spectrum. However, a combination of density functional theory (DFT) and dynamic mean field theory (DMFT) provides a natural way to improve on both these pictures.

Figures 1c-e summarize our key findings for the electron-doped iron arsenide superconductor  $\text{BaFe}_{1.9}\text{Ni}_{0.1}\text{As}_2$  and the comparison with the spin waves in  $\text{BaFe}_2\text{As}_2$ . The data points in Figs. 1c and 1d show the dispersion of spin excitations for optimal doped  $\text{BaFe}_{1.9}\text{Ni}_{0.1}\text{As}_2$  along  $[1, K]$  and  $[H, 0]$ , and the solid lines show the fit of  $\text{BaFe}_2\text{As}_2$  spin waves to an effective Heisenberg  $J_{1a} - J_{1b} - J_2$  model with  $J_{1a} \neq J_{1b}$  [13]. Figure 1e shows the local dynamic susceptibility per formula unit (f.u.), which contains two Fe(Ni) atoms, in absolute units, defined as  $\chi''(\omega) = \int \chi''(\mathbf{q}, \omega) d\mathbf{q} / \int d\mathbf{q}$  [12], where  $\chi''(\mathbf{q}, \omega) = (1/3)\text{tr}(\chi''_{\alpha\beta}(\mathbf{q}, \omega))$ , at different energies for  $\text{BaFe}_2\text{As}_2$  and  $\text{BaFe}_{1.9}\text{Ni}_{0.1}\text{As}_2$ . It is clear that electron doping on  $\text{BaFe}_2\text{As}_2$  only affects the low-energy spin excitations by broadening the spin waves below 80 meV, but has no impact on spin waves above 100 meV (see supplementary information). The quasiparticles that form within the spin-density-wave gap are sensitive to the Fermi surface change upon doping  $\text{BaFe}_2\text{As}_2$ , and hence the resulting low energy itinerant spin excitations substantially change, while the higher energy spin excitations are hardly affected.

To substantiate the key conclusions from the data and calculations presented in Figure 1, we show in Figure 2 the two-dimensional constant-energy ( $E$ ) images of spin excitations of  $\text{BaFe}_{1.9}\text{Ni}_{0.1}\text{As}_2$  in the  $(H, K)$  scattering plane for several Brillouin zones at 5 K. In the undoped phase, spin waves in  $\text{BaFe}_2\text{As}_2$  exhibits an anisotropy spin gap of

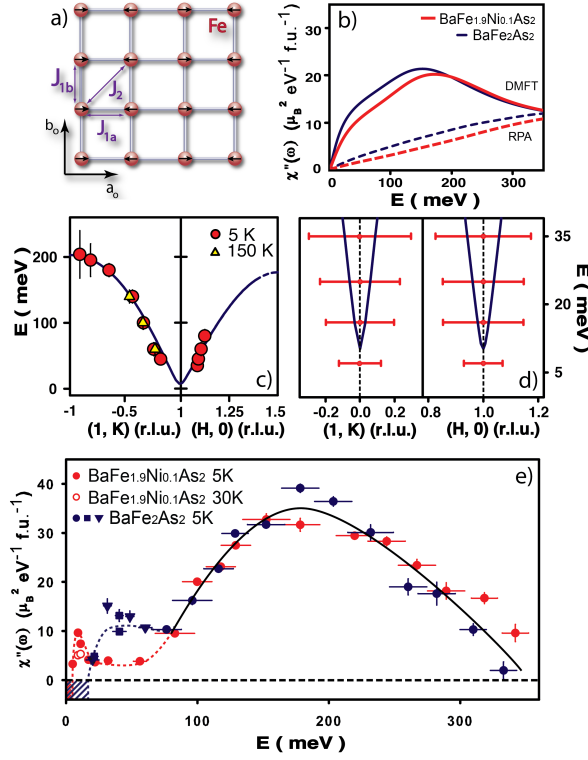


FIG. 1: Summary of neutron scattering and calculation results. Our experiments were carried out on the MERLIN time-of-flight chopper spectrometer at the Rutherford-Appleton Laboratory, UK [25]. We co-aligned 28 g of single crystals of  $\text{BaFe}_{1.9}\text{Ni}_{0.1}\text{As}_2$  (with in-plane mosaic of  $2.5^\circ$  and out-of-plane mosaic of  $4^\circ$ ). The incident beam energies were  $E_i = 20, 25, 30, 80, 250, 450, 600$  meV, and mostly with  $E_i$  parallel to the  $c$ -axis. To facilitate easy comparison with spin waves in  $\text{BaFe}_2\text{As}_2$  [13], we defined the wave vector  $Q$  at  $(q_x, q_y, q_z)$  as  $(H, K, L) = (q_x a/2\pi, q_y b/2\pi, q_z c/2\pi)$  reciprocal lattice units (rlu) using the orthorhombic unit cell, where  $a = b = 5.564$  Å, and  $c = 12.77$  Å. The data are normalized to absolute units using a vanadium standard [13], which may have a systematic error up to 20% due to differences in neutron illumination of vanadium and sample, and time-of-flight instruments. (a) AF spin structure of  $\text{BaFe}_2\text{As}_2$  with Fe spin ordering. The effective magnetic exchange couplings along different directions are depicted. (b) RPA and LDA+DMFT calculations of  $\chi''(\omega)$  in absolute units for  $\text{BaFe}_2\text{As}_2$  and  $\text{BaFe}_{1.9}\text{Ni}_{0.1}\text{As}_2$ . (c) The solid lines show spin wave dispersions of  $\text{BaFe}_2\text{As}_2$  for  $J_{1a} \neq J_{1b}$  along the  $[1, K]$  and  $[H, 0]$  directions obtained in Ref. [13]. The filled circles and upper triangles are spin excitation dispersions of  $\text{BaFe}_{1.9}\text{Ni}_{0.1}\text{As}_2$  at 5 K and 150 K, respectively. (d) The solid line shows low energy spin waves of  $\text{BaFe}_2\text{As}_2$ . The horizontal bars show the full-width-half-maximum of spin excitations in  $\text{BaFe}_{1.9}\text{Ni}_{0.1}\text{As}_2$  and above (open red circles) and below (filled blue circles)  $T_c$ . The solid and dashed lines are guide to the line. The vertical error bars indicate the statistical errors of one standard deviation. The horizontal error bars in (e) indicate energy integration range.

$\Delta = 9.8$  meV [26]. On doping, the anisotropy spin gap disappears and spin excitations form transversely elongated ellipses that decrease in intensity with increasing energy [12, 21]. For energy transfers of  $E = 10 \pm 3$  (Fig. 2a),  $33 \pm 3$  (Fig. 2b),  $43 \pm 3$  (Fig. 2c),  $60 \pm 10$  (Fig. 2d), and  $81 \pm 10$  meV (Fig. 2e), spin excitations are peaked at the AF wave vector  $Q = (1, 0)$  in the center of the Brillouin zone shown as dashed square boxes. As the energy increases to  $E = 113 \pm 10$  (Fig. 2f) and  $135 \pm 10$  meV (Fig. 2g), spin excitations start to split along the K-direction and form a ring around the  $\Gamma$  point. Finally, spin excitations near the zone boundary at  $E = 157 \pm 10$  and  $214 \pm 10$  meV form four blobs centered at  $Q = (1, 1)$ .

In order to determine the dispersion of spin excitations for  $\text{BaFe}_{1.9}\text{Ni}_{0.1}\text{As}_2$ , we cut through the two-dimensional images similar to Fig. 2 along the  $[1, K]$  and  $[H, 0]$  directions. Figures 3a-3f show constant-energy cuts along the  $[1, K]$  direction for  $E = 25 \pm 5, 55 \pm 5, 95 \pm 10, 125 \pm 10, 150 \pm 10,$  and  $210 \pm 10$  meV. The scattering becomes dispersive for spin excitation energies above 95 meV. Figures 3g-3i show similar constant-energy cuts along the  $[H, 0]$  direction. The solid lines in the Figure show identical spin wave cuts for  $\text{BaFe}_2\text{As}_2$  [13]. Since both measurements were taken in absolute units, we can compare the impact of electron-doping on the spin waves in  $\text{BaFe}_2\text{As}_2$ . At  $E = 25 \pm 5$  meV, spin excitations in superconducting  $\text{BaFe}_{1.9}\text{Ni}_{0.1}\text{As}_2$  are considerably broader in momentum space and weaker in intensity than spin waves (Figs. 3a and 3g). Upon increasing the excitation energy to  $55 \pm 5$  meV, the

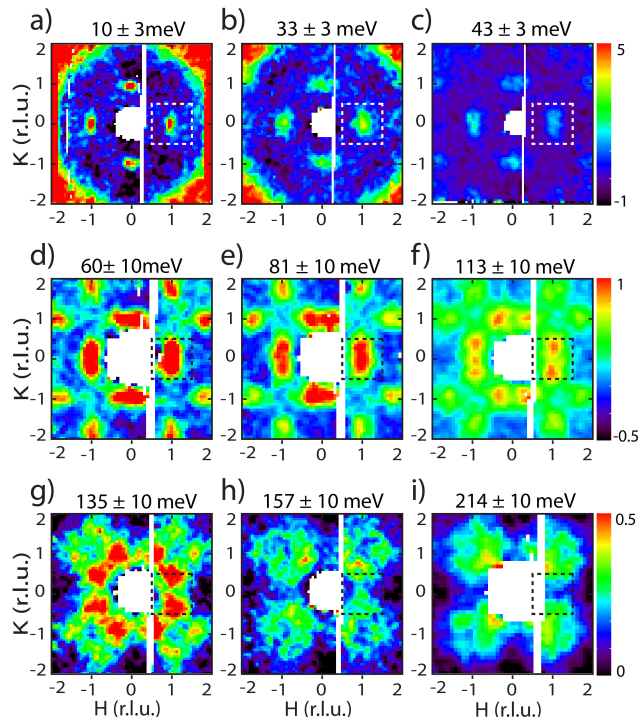


FIG. 2: Constant-energy slices through the magnetic excitations of  $\text{BaFe}_{1.9}\text{Ni}_{0.1}\text{As}_2$  at different energies in several Brillouin zones. The images were obtained after subtracting the background integrated from  $1.8 < H < 2.2$  and  $-0.2 < K < 0.2$ . The color bars represent the vanadium normalized absolute spin excitation intensity in the units of  $\text{mbarn}/\text{sr}/\text{meV}/\text{f.u}$  and the dashed boxes indicate AF zone boundaries for a single FeAs layer. Two dimensional images of spin excitations at (a)  $E = 10 \pm 3$ , (b)  $33 \pm 3$ , (c)  $43 \pm 3$ , (d)  $60 \pm 10$ , (e)  $81 \pm 10$ , (f)  $113 \pm 10$ , (g)  $135 \pm 10$ , (h)  $157 \pm 10$ , and (i)  $214 \pm 10$  meV.

dispersive spin waves in  $\text{BaFe}_2\text{As}_2$  become weaker and broader (Figs. 3b and 3h). For energies above 95 meV, spin excitations in  $\text{BaFe}_{1.9}\text{Ni}_{0.1}\text{As}_2$  are almost indistinguishable from spin waves in  $\text{BaFe}_2\text{As}_2$  in both the linewidths and intensity (Figs. 3c-3f, and 3i). Based on these constant-energy cuts, we show in Figs. 1c and 1d the comparison of spin excitation dispersions of  $\text{BaFe}_{1.9}\text{Ni}_{0.1}\text{As}_2$  (filled circles and horizontal bars) with those of spin waves in  $\text{BaFe}_2\text{As}_2$  (solid lines). Inspection of Figs. 1-3 reveals that electron-doping to  $\text{BaFe}_2\text{As}_2$  only broadens and suppresses low energy spin excitations and has no influence for spin waves above 100 meV (see supplementary information).

To reveal further the effect of electron doping on spin waves of  $\text{BaFe}_2\text{As}_2$ , we show in Figures 4a-4d constant- $Q$  cuts at different wave vectors along the  $[1, K]$  direction for spin excitations in  $\text{BaFe}_{1.9}\text{Ni}_{0.1}\text{As}_2$ . Near the Brillouin zone center at  $Q = (1, 0.05)$  and  $(1, 0.2)$ , well-defined spin excitations are observed near  $E = 40$ , and 60 meV as shown in Figs. 4a and 4b, respectively. The intensity of the scattering from the spin excitations in  $\text{BaFe}_{1.9}\text{Ni}_{0.1}\text{As}_2$  is, however, much lower than that of  $\text{BaFe}_2\text{As}_2$  shown as solid lines in the Figures. On increasing the wave vectors to  $Q = (1, 0.35)$  and  $(1, 0.5)$ , the magnetic scattering peak near  $E = 100$ , and 120 meV, and are essentially indistinguishable from spin waves in  $\text{BaFe}_2\text{As}_2$  as shown in Figs. 4c and 4d. Furthermore, spin excitations have virtually no temperature dependence between 5 K and 150 K (Fig. 4b).

Finally, we show in Figs. 4e and 4f temperature dependence of spin excitations at energies near the neutron spin resonance  $E = 9$  meV [20, 22] and at  $E = 90 \pm 5$  meV, respectively. While the intensity of the resonance at  $E = 9$  meV increases dramatically below  $T_c$ , consistent with earlier work [20, 22], spin excitations at  $90 \pm 5$  meV are identical on cooling from 150 K to 5 K. We note that high-energy spin waves in  $\text{BaFe}_2\text{As}_2$  are also weakly temperature dependent [13]. Figure 4g shows the energy dependence of the dynamic spin-spin correlation lengths, which are about  $\xi \approx 14$  Å and excitation energy independent. For comparison, the dynamic spin-spin correlation length (the solid line in Fig. 4g) in  $\text{BaFe}_2\text{As}_2$  decreases with increasing energy and becomes similar to that of  $\text{BaFe}_{1.9}\text{Ni}_{0.1}\text{As}_2$  for excitation energies above 100 meV.

To check if spin excitations in the AF  $\text{BaFe}_2\text{As}_2$  and superconducting  $\text{BaFe}_{1.9}\text{Ni}_{0.1}\text{As}_2$  can be understood in an itinerant picture, we calculate the local susceptibility  $\chi''(\omega)$  using the random phase approximation (RPA) based on realistic Fermi surfaces and band structures [27]. Within RPA, the polarization bubble  $\chi^0$  is computed from the density function theory (DFT) Kohn-Sham Green's functions while the irreducible vertex  $\Gamma^{irr}$  is approximated by the

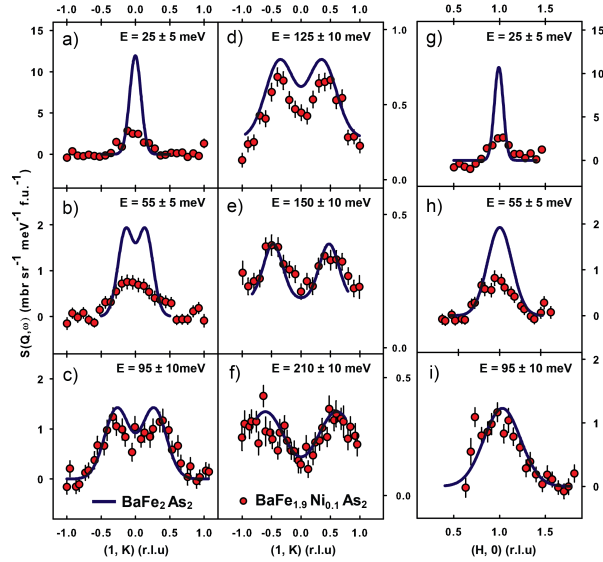


FIG. 3: Constant-energy cuts of the spin excitation dispersion as a function of increasing energy along the  $[1, K]$  and  $[H, 0]$  directions for  $\text{BaFe}_{1.9}\text{Ni}_{0.1}\text{As}_2$ . The solid lines show identical cuts for spin waves of  $\text{BaFe}_2\text{As}_2$  in absolute units. (a) Constant-energy cut along the  $[1, K]$  direction at  $E = 25 \pm 5$ , (b)  $55 \pm 5$ , (c)  $95 \pm 10$ , (d)  $125 \pm 10$ , (e)  $150 \pm 10$ , and (f)  $210 \pm 10$  meV. (g) Constant-energy cut along the  $[H, 0]$  direction at  $E = 25 \pm 5$ , (h)  $55 \pm 5$ , and  $95 \pm 10$  meV. The error bars indicate the statistical errors of one standard deviation.

screened Coulomb parameters  $\tilde{U}$  and  $\tilde{J}$ . Using  $\tilde{U} = 1.3$  eV and  $\tilde{J} = 0.4$  eV and performing calculations above  $T_N$  [27], we find that the RPA estimated  $\chi''(\omega)$  for  $\text{BaFe}_2\text{As}_2$  and  $\text{BaFe}_{1.9}\text{Ni}_{0.1}\text{As}_2$  (solid and dashed lines in Fig. 1b) increases approximately linearly with energy and has absolute values about a factor of three smaller than the observation (Fig. 1e). Although the RPA calculation depends on Coulomb parameters used, we note that the 5-orbital Hubbard model calculation using  $\tilde{U} = 0.8$  eV and  $\tilde{J} = 0.2$  eV produces essentially similar local magnetic spectra [28]. Therefore, a pure RPA type itinerant model underestimates the absolute spectral weight of the magnetic excitations in iron pnictides.

The solid blue and red lines in Fig. 1b show the calculated local susceptibility using a combined DFT and DMFT in the paramagnetic state. Within DFT+DMFT,  $\chi''(\mathbf{q}, \omega)$  is computed by the Bethe-Salpeter equation using the polarization function  $\chi^0$  and the two-particle local irreducible vertex function  $\Gamma^{irr}$  [27].  $\chi^0$  is computed from the interacting one-particle Green's function determined by the charge self-consistent full potential DFT+DMFT method and  $\Gamma^{irr}$  is extracted from the two particle vertex function of the auxiliary impurity problem. The latter is defined by the DMFT procedure using projection of all electronic states to the  $d$  character within the iron muffin-tin sphere. By comparing DFT+DMFT and RPA calculations in Fig. 1b with data in Fig. 1e, we see that the former is much closer to the observation. Note that the calculation is done in the paramagnetic state, hence the low energy modifications of the spectra due to the long range AF order is not captured in this calculation. RPA can describe only the itinerant part of the electron spectra, while DFT+DMFT captures the essential aspects of both the quasiparticles and the iron local moments formed by strong Hunds coupling (see supplementary information for more detailed discussion). The improved agreement of DFT+DMFT thus suggest that both the quasiparticles and the local moment aspects of the iron electrons are needed to obtain the correct intensity and energy distribution of neutron scattering spectra [27].

One way to quantitatively compare spin excitations in iron pnictides with those in copper oxides is to estimate their total fluctuating moments, defined as  $\langle m^2 \rangle = (3\hbar/\pi) \int \chi''(\omega) d\omega / (1 - \exp(-\hbar\omega/kT))$  [12]. Based on Fig. 1e, we find that  $\langle m^2 \rangle = 3.17 \pm 0.16$  and  $3.2 \pm 0.16 \mu_B^2$  per Fe(Ni) for  $\text{BaFe}_2\text{As}_2$  and  $\text{BaFe}_{1.9}\text{Ni}_{0.1}\text{As}_2$ , respectively. Using the formula for magnetic moment of a spin  $\langle m^2 \rangle = (g\mu_B)^2 S(S+1)$  (where  $g = 2$ ) [29], we find an effective iron spin  $S$  of about  $1/2$ , similar to that of  $\text{CaFe}_2\text{As}_2$  [30]. These results also show that superconductivity in electron-doped system hardly changes the total size of the fluctuating moment. In the fully localized (insulating) case, the formal  $\text{Fe}^{2+}$  oxidation state in  $\text{BaFe}_2\text{As}_2$  would give a  $3d^6$  electronic configuration. Hund's rules would yield  $S = 2$  and  $\langle m^2 \rangle = 24 \mu_B^2$  per Fe. This is considerable more than the observed values suggesting that significant hybridization of Fe  $3d$  with pnictide  $p$  orbitals and among themselves, which leads to a metallic state where the Hund's coupling is less important than in the atomic limit [31]. For comparison, we note that  $\langle m^2 \rangle > 1.9 \mu_B^2$  per Cu for the AF insulating  $\text{La}_2\text{CuO}_4$  measured over a similar energy range [14, 15]. From Fig. 1e, we see that the large fluctuating

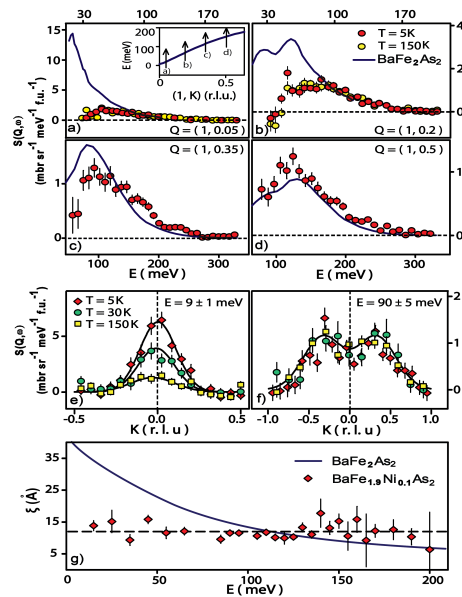


FIG. 4: Constant-Energy/wave vector ( $Q$ ) dependence of the spin excitations and dynamic spin-spin correlation lengths for  $\text{BaFe}_{1.9}\text{Ni}_{0.1}\text{As}_2$  and  $\text{BaFe}_2\text{As}_2$ . (a)-(d) Constant- $Q$  cuts at  $Q = (1, 0.05)$ ,  $(1, 0.2)$ ,  $(1, 0.35)$ , and  $(1, 0.5)$ , respectively, at  $T = 5$  K (solid red circles) and 150 K (yellow filled circles) with background at  $Q = (2, 0)$  subtracted. The negative scattering in the data are due to over subtraction of the phonon background. The solid lines are identical cuts from spin waves in  $\text{BaFe}_2\text{As}_2$ . For excitations below 100 meV, the intensity of the scattering of  $\text{BaFe}_{1.9}\text{Ni}_{0.1}\text{As}_2$  is suppressed compared to that of  $\text{BaFe}_2\text{As}_2$ . For energies above 100 meV, the magnetic scattering is virtually identical between the parent and superconductor. (e) Constant-energy cuts at the neutron spin resonance energy of  $E = 9 \pm 1$  meV [20] below and above  $T_c$ . The solid lines are Gaussian fits on linear backgrounds. (f) Temperature dependence of spin excitations at  $E = 90 \pm 5$  meV. (g) Energy dependence of the dynamic spin-spin correlation lengths ( $\xi$ ) at 5 K obtained by Fourier transform of constant-energy cuts similar to those in Fig. 3a-f and Fig. 4e,f. For all excitation energies probed ( $10 \leq E \leq 200$  meV), the dynamic spin-spin correlation lengths are independent of energy. The solid line shows energy dependence of  $\xi$  for  $\text{BaFe}_2\text{As}_2$ . The error bars indicate the statistical errors of one standard deviation.

moment  $\langle m^2 \rangle$  in iron pnictides arises mostly from high-energy spin excitations that is essentially temperature [13] and electron-doping independent within the errors of our measurements (Fig. 1). Since there are currently no high-energy spin excitation data in absolute units for optimally hole-doped  $\text{Ba}_{0.67}\text{K}_{0.33}\text{Fe}_2\text{As}_2$  [32], it is unclear how hole-doping  $\text{BaFe}_2\text{As}_2$  modifies the spin-wave spectra.

The DFT+DMFT calculation suggests that both the band structure and the local moment aspects (e.g. Hund's coupling) of the iron electrons are needed to obtain a good description of the magnetic response in  $\text{BaFe}_2\text{As}_2$  and  $\text{BaFe}_{1.9}\text{Ni}_{0.1}\text{As}_2$ . The weak electron-doping dependence of the fluctuating moment is consistent with the Hund's metal picture, where electron filling associated with the Fe  $3d^6$  electrons by Ni-doping is not expected to drastically affect the local moments. What is surprising is that the similarities in the local susceptibilities of the iron pnictides studied here and the parents of the cuprate superconductors. The large fluctuating moment, arising from Hund's rule coupling, and concentrated at higher energy in iron pnictides, nevertheless gives an imprint on the massive and anisotropic low-energy quasiparticles [33], which form Cooper pairs at low energy. This physics is different from the physics of doped charge transfer insulators appropriate for copper oxides [10], hence the electron correlations in iron pnictides and copper oxides have different microscopic origins, although they are important for understanding the magnetism and superconductivity for both materials.

- 
- [1] Kamihara, Y., Watanabe, T., Hirano, M. & Hosono, H. Iron-based layered superconductor  $\text{La}[\text{O}_{1-x}\text{F}_x]\text{FeAs}$  ( $x = 0.05-0.12$ ) with  $T_c = 26$  K. *J. Am. Chem. Soc.* **130**, 3296-3297 (2008).
  - [2] de la Cruz, C. *et al.*, Magnetic order close to superconductivity in the iron-based layered  $\text{LaO}_{1-x}\text{F}_x\text{FeAs}$  systems. *Nature* **453**, 899-902 (2008).
  - [3] Paglione, J. & Greene, R. L., High-temperature superconductivity in iron-based materials. *Nat. Phys.* **6**, 645-658 (2010).
  - [4] Mazin, I. I., Singh, D. J., Johannes, M. D., & Du, M. H., Unconventional superconductivity with a sign reversal in the

- order parameter of  $\text{LaFeAsO}_{1-x}\text{F}_x$ . Phys. Rev. Lett. **101**, 057003 (2008).
- [5] Dong, J., *et al.*, Competing orders and spin-density-wave instability in  $\text{LaO}_{1-x}\text{F}_x\text{FeAs}$ . Europhys. Lett. **83**, 27006 (2008).
- [6] Fawcett, E., Spin-density-wave antiferromagnetism in chromium, Rev. Mod. Phys. **60**, 209-283 (1998).
- [7] Haule, K., Shim, J. H., & Kotliar, G., Correlated electronic structure of  $\text{LaO}_{1-x}\text{F}_x\text{FeAs}$ . Phys. Rev. Lett. **100**, 226402 (2008).
- [8] Si, Q. & Abrahams, E., Strong correlations and magnetic frustration in the high  $T_c$  iron pnictides. Phys. Rev. Lett. **101**, 076401 (2008).
- [9] Xu, C. K., Müller, & Sachdev, S., Ising and spin orders in the iron-based superconductors. Phys. Rev. B **78**, 020501(R) (2008).
- [10] Lee, P. A., Nagaosa, N. & Wen, X.-G., Doping a Mott insulator: Physics of high-temperature superconductivity. Rev. Mod. Phys. **78**, 17-85 (2006).
- [11] Inosov, D. S., *et al.*, Normal-state spin dynamics and temperature-dependent spin-resonance energy in optimally doped  $\text{BaFe}_{1.85}\text{Co}_{0.15}\text{As}_2$ . Nat. Phys. **6**, 178-181 (2010).
- [12] Lester, C. *et al.*, Dispersive spin fluctuations in the nearly optimally doped superconductor  $\text{Ba}(\text{Fe}_{1-x}\text{Co}_x)_2\text{As}_2$  ( $x = 0.065$ ). Phys. Rev. B **81**, 064505 (2010).
- [13] Harriger, L. W. *et al.*, Nematic spin fluid in the tetragonal phase of  $\text{BaFe}_2\text{As}_2$ . Phys. Rev. B **84**, 054544 (2011).
- [14] Headings, N. S., Hayden, S. M., Coldea, R., & Perring, T. G., Anomalous high-energy spin excitations in the high- $T_c$  superconductor-parent antiferromagnet  $\text{La}_2\text{CuO}_4$ . Phys. Rev. Lett. **105**, 247001 (2010).
- [15] Hayden, S. M. *et al.*, Comparison of the high-frequency magnetic fluctuations in insulating and superconducting  $\text{La}_{2-x}\text{Sr}_x\text{CuO}_4$ . Phys. Rev. Lett. **76**, 1344-1347 (1996).
- [16] Basov, D. N. & Chubukov, A. V., Manifesto for a higher  $T_c$ , Nature Physics **7**, 272-276 (2011).
- [17] Huang, Q. *et al.*, Neutron-diffraction measurements of magnetic order and a structural transition in the parent  $\text{BaFe}_2\text{As}_2$  compound of FeAs-based high-temperature superconductors. Phys. Rev. Lett. **101**, 257003 (2008).
- [18] Lester, C. *et al.*, Neutron scattering study of the interplay between structure and magnetism in  $\text{Ba}(\text{Fe}_{1-x}\text{Co}_x)_2\text{As}_2$ . Phys. Rev. B **79**, 144523 (2009).
- [19] Lumsden, M. D. *et al.*, Two-dimensional resonant magnetic excitation in  $\text{BaFe}_{1.84}\text{Co}_{0.16}\text{As}_2$ . Phys. Rev. Lett. **102**, 107005 (2009).
- [20] Chi, S. *et al.*, Inelastic neutron-scattering measurements of a three-dimensional spin resonance in the FeAs-based  $\text{BaFe}_{1.9}\text{Ni}_{0.1}\text{As}_2$  superconductor. Phys. Rev. Lett. **102**, 107006 (2009).
- [21] Li, H. F. *et al.*, Anisotropic and quasipropagating spin excitations in superconducting  $\text{Ba}(\text{Fe}_{0.926}\text{Co}_{0.074})_2\text{As}_2$ . Phys. Rev. B **82**, 140503(R) (2010).
- [22] Wang, M. Y. *et al.*, Electron-doping evolution of the low-energy spin excitations in the iron arsenide superconductor  $\text{BaFe}_{2-x}\text{Ni}_x\text{As}_2$ . Phys. Rev. B **81**, 174524 (2010).
- [23] Chen, Y. C., Lu, X. Y., Wang, M., Luo, H. Q., & Li, S. L., Systematic growth of  $\text{BaFe}_{2-x}\text{Ni}_x\text{As}_2$  large crystals. Supercond. Sci. Technol. **24**, 065004 (2011).
- [24] Bud'ko, S. L., Ni, N., & Canfield, P. C., Jump in specific heat at the superconducting transition temperature in  $\text{Ba}(\text{Fe}_{1-x}\text{Co}_x)_2\text{As}_2$  and  $\text{Ba}(\text{Fe}_{1-x}\text{Ni}_x)_2\text{As}_2$  single crystals. Phys. Rev. B **79**, 220516(R) (2009).
- [25] Bewley, R. I. *et al.*, MERLIN, a new high count rate spectrometer at ISIS. Physica B **385-386**, 1029-1031 (2006).
- [26] Matan, K., Morinaga, R., Lida, K., & Sato, T. J., Anisotropic itinerant magnetism and spin fluctuations in  $\text{BaFe}_2\text{As}_2$ : A neutron scattering study. Phys. Rev. B **79**, 054526 (2009).
- [27] Park, H., Haule, K., & Kotliar, G., Magnetic excitation spectra in  $\text{BaFe}_2\text{As}_2$ : a two-particle approach within a combination of the density functional theory and the dynamical mean-field theory method. Phys. Rev. Lett. **107**, 137007 (2011).
- [28] Graser, S. *et al.*, Spin fluctuations and superconductivity in a three-dimensional tight-binding model for  $\text{BaFe}_2\text{As}_2$ . Phys. Rev. B **81**, 214503 (2010).
- [29] Lorenzana, J., Seibold, G., & Coldea, R., Sum rules and missing spectral weight in magnetic neutron scattering in the cuprates. Phys. Rev. B **72**, 224511 (2005).
- [30] Zhao, J. *et al.*, Spin waves and magnetic exchange interactions in  $\text{CaFe}_2\text{As}_2$ . Nat. Phys. **5**, 555-560 (2009).
- [31] Cvetkovic, V. & Tesanovic, Z., Multiband magnetism and superconductivity in Fe-based compounds. Europhys. Lett. **85**, 37002 (2009).
- [32] Zhang, C. L. *et al.*, Neutron Scattering Studies of spin excitations in hole-doped  $\text{Ba}_{0.67}\text{K}_{0.33}\text{Fe}_2\text{As}_2$  superconductor. Scientific Reports **1**, 115 (2011).
- [33] Yin, Z. P., Haule, K. & Kotliar, G., Magnetism and charge dynamics in iron pnictides. Nat. Phys. **7**, 294-297 (2011).

**Acknowledgements** We thank T. A. Maier, J. P. Hu, and Tao Xiang for helpful discussions. The work at UTK is supported by the U.S. NSF-DMR-1063866 and NSF-OISE-0968226. Work at IOP is supported by the MOST of China 973 programs (2012CB821400, 2011CBA00110) and NSFC-11004233. The work at Rutgers is supported by DOE BES DE-FG02-99ER45761 (GK), ACS Petroleum Research Fund 48802 and Alfred P. Sloan foundation (KH).

**Author contributions** P.D. and M.S.L. planned neutron scattering experiments. M.S.L., L.W.H., H.Q.L., R.A.E., T.G., and P.D. carried out neutron scattering experiments. Data analysis was done by M.S.L. with help from L.W.H., R.A.E., T.G., and S.M.H. The samples were grown by H.Q.L. and co-aligned by M.S.L. and M.W. The DFT and DMFT calculations were done by H.P., K.H., and G.K. The paper was written by P.D., K.H., and G.K. with input from S.M.H. and M.S.L. All coauthors provided comments on the paper.

**Additional information** The authors declare no competing financial interests. Supplementary information accompanies this paper on [www.nature.com/naturephysics](http://www.nature.com/naturephysics). Reprints and permissions information is available online at <http://www.nature.com/reprints>. Correspondence and requests for materials should be addressed to P.D.

# Nature of magnetic excitations in superconducting BaFe<sub>1.9</sub>Ni<sub>0.1</sub>As<sub>2</sub>

Mengshu Liu, Leland W. Harriger, Huiqian Luo, Meng Wang, R. A. Ewings, T. Guidi, Hyowon Park, Kristjan Haule, Gabriel Kotliar, S. M. Hayden, and Pengcheng Dai

Our BaFe<sub>2-x</sub>Ni<sub>x</sub>As<sub>2</sub> electron-doped samples were grown using self flux method as described before [1]. Since the electronic and superconducting properties of Co and Ni-doping of BaFe<sub>2</sub>As<sub>2</sub> near optimal superconducting transition temperatures are almost identical [2], we chose to study spin excitations in optimally doped BaFe<sub>1.9</sub>Ni<sub>0.1</sub>As<sub>2</sub> with  $T_c = 20$  K. To further compare spin excitations in BaFe<sub>2</sub>As<sub>2</sub> and BaFe<sub>1.9</sub>Ni<sub>0.1</sub>As<sub>2</sub>, we show in Figure 1 spin excitations of these two materials at different energies. Consistent with data shown in Figs. 2-4 of the main text, we see that the effect of electron-doping is to mostly modify spin excitations below 80 meV.

Our theoretical method for computing the magnetic excitation spectrum employs abinitio full potential DFT+DMFT method, as implemented in Ref. [3], which is based on the commercial DFT code of Wien2k [4]. The DMFT method requires solution of the generalized quantum impurity problem, which is here solved by the numerically exact continuous-time quantum Monte Carlo method (CTQMC) [5, 6]. The Coulomb interaction matrix for electrons on iron atom was determined by the self-consistent GW method in Ref. [7], giving  $U = 5$  eV and  $J = 0.8$  eV for the local basis functions within the all electron approach employed in our DFT+DMFT method.

The dynamical magnetic susceptibility  $\chi(\mathbf{q}, \omega)$  is computed from the *ab initio* perspective by extracting the two-particle vertex functions of DFT+DMFT solution  $\Gamma_{loc}^{irr}$ . The polarization bubble  $\chi^0$  is computed from the fully interacting one particle Greens function. The full susceptibility is computed from  $\chi^0$  and the two-particle irreducible vertex function  $\Gamma_{loc}^{irr}$ , which is assumed to be local in the same basis in which the DMFT self-energy is local, implemented here by the projector to the muffin-tin sphere [3]. In order to extract  $\Gamma_{loc}^{irr}$ , we employ the Bethe-Salpeter equation (see Fig. 2) which relates the local two-particle Green's function ( $\chi_{loc}$ ), sampled by CTQMC, with both the local polarization function ( $\chi_{loc}^0$ ) and  $\Gamma_{loc}^{irr}$ :

$$\Gamma_{loc}^{irr}{}_{\alpha_3\sigma_3, \alpha_4\sigma_4}^{\alpha_1\sigma_1, \alpha_2\sigma_2}(i\nu, i\nu')_{i\omega} = \frac{1}{T} [(\chi_{loc}^0)_{i\omega}^{-1} - \chi_{loc}^{-1}]. \quad (1)$$

$\Gamma_{loc}^{irr}$  depends on three Matsubara frequencies ( $i\nu, i\nu'; i\omega$ ), and both the spin ( $\sigma_{1-4}$ ) and the orbital ( $\alpha_{1-4}$ ) indices, which run over  $3d$  states on the iron atom.  $T$  is the temperature.

Once the irreducible vertex  $\Gamma_{loc}^{irr}$  is obtained, the momentum dependent two-particle Green's function is constructed again using the Bethe-Salpeter equation (Fig. 2) by replacing the local polarization function  $\chi_{loc}^0$  by the non-local one  $\chi_{\mathbf{q}, i\omega}^0$ :

$$\chi_{\alpha_3\sigma_3, \alpha_4\sigma_4}^{\alpha_1\sigma_1, \alpha_2\sigma_2}(i\nu, i\nu')_{\mathbf{q}, i\omega} = [(\chi^0)_{\mathbf{q}, i\omega}^{-1} - T \cdot \Gamma_{loc}^{irr}]^{-1}. \quad (2)$$

Finally, the dynamic magnetic susceptibility  $\chi(\mathbf{q}, i\omega)$  is obtained by closing the two particle green's function with the magnetic moment  $\mu = \mu_B(\mathbf{L} + 2\mathbf{S})$  vertex, and summing over all internal degrees of freedom, i.e., orbitals ( $\alpha_{1-4}$ ), spins ( $\sigma_{1-4}$ ) and frequencies ( $i\nu, i\nu'$ ), on the four external legs

$$\chi(\mathbf{q}, i\omega) = T \sum_{i\nu, i\nu'} \sum_{\substack{\alpha_1\alpha_2 \\ \alpha_3\alpha_4}} \sum_{\substack{\sigma_1\sigma_2 \\ \sigma_3\sigma_4}} \mu_{\alpha_3\sigma_3}^z \mu_{\alpha_4\sigma_4}^z \chi_{\alpha_3\sigma_3, \alpha_4\sigma_4}^{\alpha_1\sigma_1, \alpha_2\sigma_2}(i\nu, i\nu')_{\mathbf{q}, i\omega} \quad (3)$$

We note that the same abinitio methodology which is here used to compute the magnetic excitation spectra, was previously shown to describe the photoemission, the optical spectra and the magnetic moments of this material [8] in excellent agreement with experiment.

- 
- [1] Chen, Y. C., Lu, X. Y., Wang, M., Luo, H. Q., & Li, S. L., Systematic growth of BaFe<sub>2-x</sub>Ni<sub>x</sub>As<sub>2</sub> large crystals. *Supercond. Sci. Technol.* **24**, 065004 (2011).  
 [2] Bud'ko, S. L., Ni, N., & Canfield, P. C., Jump in specific heat at the superconducting transition temperature in Ba(Fe<sub>1-x</sub>Co<sub>x</sub>)<sub>2</sub>As<sub>2</sub> and Ba(Fe<sub>1-x</sub>Ni<sub>x</sub>)<sub>2</sub>As<sub>2</sub> single crystals. *Phys. Rev. B* **79**, 220516(R) (2009).  
 [3] Haule, K., Yee, C.-H., Kim, K., Dynamical mean-field theory within the full-potential methods: Electronic structure of CeIrIn<sub>5</sub>, CeCoIn<sub>5</sub>, and CeRhIn<sub>5</sub>. *Phys. Rev. B* **81**, 195107 (2010).



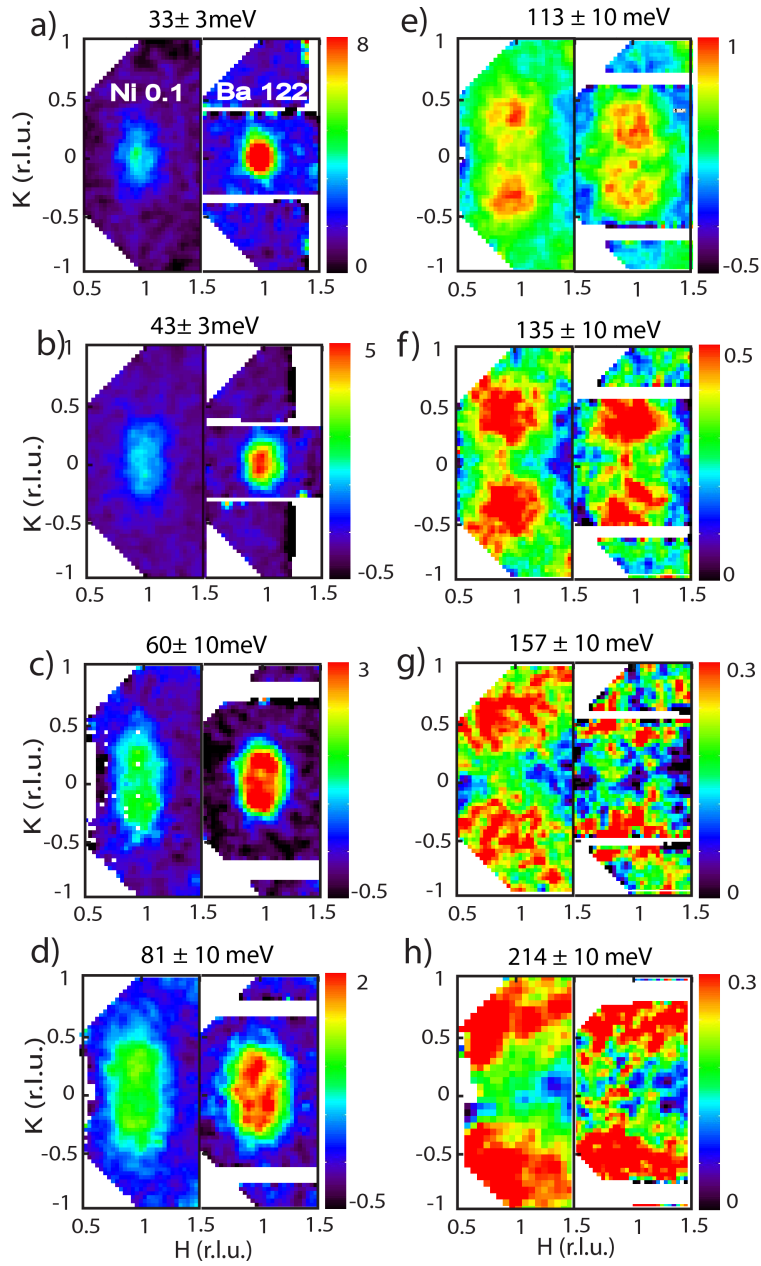


Figure 1: Constant-energy images of the spin excitations as a function of increasing energy for  $\text{BaFe}_{1.9}\text{Ni}_{0.1}\text{As}_2$  and  $\text{BaFe}_2\text{As}_2$  in units of  $\text{mbarns/sr/meV/f.u.}$  (a)  $E = 33 \pm 3$ , (b)  $43 \pm 3$ , (c)  $60 \pm 10$ , (d)  $81 \pm 10$ , (e)  $113 \pm 10$ , (f)  $135 \pm 10$ , (g)  $157 \pm 10$ , and (h)  $214 \pm 10$  meV.

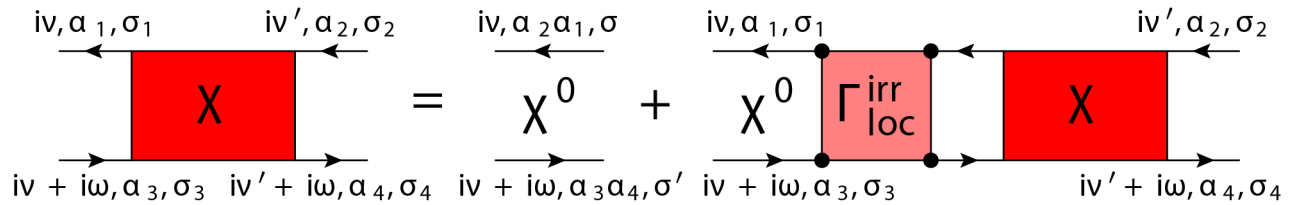


Figure 2: The Feynman diagrams for the Bethe-Salpeter equation. It relates the two-particle Green's function ( $\chi$ ) with the polarization ( $\chi^0$ ) and the local irreducible vertex function ( $\Gamma_{loc}^{irr}$ ). The non-local two-particle Green's function is obtained by replacing the local propagator by the non-local propagator.

- [4] Blaha, P., Schwarz, K., Madsen, G. K. H., Kvasnicka, K., & Luitz, J., Wien2K, Karlheinz Schwarz, Technische Universitat Wien, Austria (2001).
- [5] Haule, K., Quantum Monte Carlo impurity solver for cluster dynamical mean-field theory and electronic structure calculations with adjustable cluster base. *Phys. Rev. B* **75**, 155113 (2007).
- [6] Werner, P., Comanac, A., de' Medici, L., Troyer, M., & Millis, A. J., Continuous-Time Solver for Quantum Impurity Models. *Phys. Rev. Lett.* **97**, 076405 (2006).
- [7] Kutepov, A., Haule, K., Savrasov, S. Y., & Kotliar, G., Self-consistent *GW* determination of the interaction strength: Application to the iron arsenide superconductors. *Phys. Rev. B* **82**, 045105 (2010).
- [8] Yin, Z. P., Haule, K., & Kotliar, G., Magnetism and charge dynamics in iron pnictides. *Nature Physics* **7**, 294-297 (2011).